Article

Sustainable Activated Carbon Production from Sunflower Seeds via Chemical Activation

Selma Kuloglija *, Amal El Gohary Ahmed, Christian Jordan, Matthias Golda, Wolfgang Impsmiller, Noah Steinacher, Franz Winter, Daniela Meitner, Angelika Luckeneder, Michael Harasek

Posted Date: 14 February 2025

doi: 10.20944/preprints202502.1032.v1

Keywords: biochar; KOH activation; activated carbon; chemical activation; sustainable materials; environmental remediation

Article

Sustainable Activated Carbon Production from Sunflower Seeds via Chemical Activation

Selma Kuloglija [1,*], Amal Ahmed El Gohary [1], Christian Jordan [1], Matthias Golda [1], Wolfgang Ipsmiller [1], Noah Steinacher [1], Franz Winter [1], Daniela Meitner [2], Angelika Luckeneder [2] and Michael Harasek [1]

[1] Institute of Chemical, Environmental & Bioscience Engineering E166, Technische Universität Wien, 1060 Vienna, Austria

[2] Next Generation Elements GmbH, Gewerbstrasse 4, 4511 Allhaming, Austria

* Correspondence: selma.kuloglija@tuwien.ac.at (Institute of Chemical, Environmental & Bioscience Engineering E166, Technische Universität Wien, 1060 Vienna, Austria)

Abstract: The increasing demand for high-performance activated carbon necessitates applying sustainable and cost-effective production methods. This study explores the use of biochar, derived from renewable biomass. The primary feedstock for biochar consisted of woody residues from composting, along with pre-dried sunflower seed shells that had a moisture content of around 10% as a precursor for the production of activated carbon. The process started with carbonization followed by potassium hydroxide (KOH) activation, key parameters such as the impregnation ratio, temperature, and activation time were optimized to enhance the physicochemical properties of the activated carbon. Under optimized conditions, namely a KOH-to-biochar impregnation ratio of 3:1, an activation temperature of 800 °C, and an activation duration of 5 hours, the yield of activated carbon is 58% and a specific surface area of 498 m^2/g. A significant enhancement in surface area, with a maximum value of 709 m^2/g achieved after increasing the time to 24 hours of activation. differential scanning calorimetry (DSC) analysis was applied to evaluate the CO_2 adsorption performance of both biochar and activated biochar at 30°C, demonstrating a 30% improvement in adsorption efficiency following activation. This study underscores the potential of biochar as a renewable and sustainable precursor for the production of high-performance activated carbon. The findings contribute to the advancement of environmentally friendly production technologies and highlight the potential applicability of biochar-derived activated carbon in gas adsorption and environmental remediation.

Keywords: biochar; KOH activation; activated carbon; chemical activation; sustainable materials; environmental remediation

1. Introduction

Activated carbon (AC) has been known for over a hundred years as a vital material used across various industries. Its broad application stems from its unique structural properties, such as its extensive surface area and functional groups, which can be tailored based on the raw materials, activation agents, and production techniques employed [1–3]. AC is indispensable in refining processes due to its properties. In recent years, there has been a significant shift towards using sustainable and economical sources to produce activated carbon. Agricultural by-products such as peanut shells [4], bamboo [5], orange peel [6], olive [1,7], rice straw [8], chicken manure [9], and other biomass materials have become increasingly alternatives for this purpose. This approach reduces production costs and offers a greener alternative to conventional methods, making AC production more accessible and economically viable.

Biochar, produced by thermochemical pyrolysis of organic biomass, has been evaluated as a valuable precursor in the development of activated carbon. As a carbon-rich material, biochar is

 doi:10.20944/preprints202502.1032.v1

increasingly recognized for its capacity to serve as a long-term carbon storage solution, helping to mitigate greenhouse gas emissions [10], and has the potential to be used as a soil amendment, contributing to carbon sequestration while enhancing soil health. Biochar is derived from a diverse range of biomass sources, including agricultural residues (such as wheat straw, bagasse, and rice husks), woody materials, food waste, and animal manure [11].

Pyrolysis is used to convert agricultural residues into biochar to make a sustainable and profitable source material for the production of activated carbon. Biochar's properties can be tailored through modification techniques, enhancing its suitability for various applications and contributing to its environmental benefits. Converting biomass into biochar has gained momentum due to its ability to reduce CO_2 emissions during production [12,13]. Primarily, biochar was viewed as a source of renewable energy, used for generating heat and powering various processes. However, its applications have expanded in energy production [14]. Nowadays, biochar plays a crucial role in a range of sectors, including water treatment and air purification, as well as serving as a sustainable fuel alternative for cooking. Besides these applications, biochar provides environmental advantages like minimizing nitrate leaching into soils and effectively capturing both organic and inorganic pollutants [15–17]. It has also been demonstrated to lower methane and carbon emissions and offers an efficient means of removing heavy metals from stormwater runoff, further enhancing its environmental value [11]. The utility of activated carbon extends to numerous fields, including but not limited to, the purification of liquids and gases, protection against hazardous substances, recovery of solvents, and acting as a support material in catalytic processes [9]. Also, AC is increasingly being investigated for advanced applications such as energy storage [18], biomedical devices [19], and environmental remediation due to its high adsorptive capacity, which is directly linked to its internal porosity and surface characteristics. The development of high-performance activated carbon depends on several critical factors, such as the choice of precursor material, activation temperature, and the duration of the activation process [20]. Despite the availability of low-cost biomass sources, the complexity of commercial production processes can be a barrier, especially in regions with limited technological capabilities [21]. Focusing on locally available biomass can potentially address these challenges and promote wider adoption of AC technologies. Activated carbon can be produced through two methods: chemical and physical activation. Chemical activation involves treating the raw material with chemical agents at relatively low temperatures, simultaneously carbonizing and activating the material to enhance its pore structure and surface area. while physical activation is a two-step process where the material is first carbonized and then activated using gases like steam or CO_2 at higher temperatures [22–24]. Chemical activation is preferred due to its efficiency in achieving activated carbons with higher surface areas, better-developed pore structures, and higher carbon yields. This method also operates at lower temperatures and within shorter timeframes, which can be advantageous regarding energy consumption and production efficiency. Commonly utilized chemicals in this process include $ZnCl_2$ [25,26], KOH [27], H_3PO_4 [28,29], NaOH [30], Na_2CO_3 [31], H_2SO_4 [32], and K_2CO_3 [33].

Potassium hydroxide (KOH) is widely regarded in scientific literature as an exceptionally effective activating agent in producing activated carbon. Its use is particularly favored due to its ability to produce materials with significantly higher surface areas compared to other activation methods and highly microporous structures [9,23]. These characteristics are important for applications requiring superior adsorption capacities and enhanced properties of electrochemical, making KOH-activated carbon a preferred material in fields such as energy storage and environmental remediation.

One of the key advantages of KOH is its role in promoting the formation of hydroxyl (-OH) functional groups on the surface of activated carbon. These functional groups contribute to the overall reactivity and adsorption efficiency of the material. Compared to other chemical activating agents, KOH stands out because of its effectiveness in creating a well-developed pore structure [34]. This effectiveness is due to the capability of potassium to form intercalation compounds with carbon, which facilitates the expansion and opening of the carbon structure during activation. Moreover,

 doi:10.20944/preprints202502.1032.v1

KOH undergoes a series of chemical reactions that further enhance pore formation. Specifically, KOH is partially converted to potassium oxide (K_2O), which, under the presence of carbon, reduces to potassium (K). This reduction process is accompanied by carbon gasification, which results in the release of CO_2 and the creation of additional pores within the carbon matrix [34]. The cumulative influence of these reactions is the development of a highly porous and reactive activated carbon material, with properties that are often superior to those produced using other activating agents. In summary, the capability of KOH to generate activated carbon with high surface areas, rich microporosity, and excellent electrochemical properties, along with its unique chemical interactions during activation, makes it an advantageous choice for producing high-performance activated carbons.

In this study, the conversion of biochar derived from biomass into high-performance activated carbon through chemical activation using potassium hydroxide (KOH) under a nitrogen (N_2) atmosphere is investigated. This research aims to analyze the impact of KOH activation on the physical and chemical properties of biochar, including surface area, porosity, and chemical composition, to optimize the production of activated carbon with improved adsorption capabilities and to help develop sustainable, efficient, and cost-effective methods for producing activated carbon from renewable biomass sources.

2. Materials and Methods

2.1. Materials

The biochar used in the experiments was sourced from an Austrian company, Sonnenerde GmbH. The primary feedstock for its production consisted of woody residues from composting, along with pre-dried sunflower seed shells that had a moisture content of around 10%. The pyrolysis process for this feedstock was conducted using a "T-cracker" type autothermal auger reactor produced by NGE, operating at temperatures exceeding 800°C.

2.2. Determination of Particle Size Distribution

The particle size of bulk materials significantly affects various process-specific properties, necessitating the measurement of average particle size and distribution width. Laser diffraction (LD) particle size analysis was employed for biochar characterization, with samples presented as aerodispersion.

2.2.1. Sample Preparation

The biochar sample, stored dry and protected from sunlight, was gently shaken for homogeneity, and a representative 30 g mixed sample was extracted. This sample was divided into three aliquots of approximately 10 g each: the first for instrument parameter adjustment and the second and third for particle size analysis.

2.2.2. Instrumental Analysis

LD analysis used a Malvern Instruments Mastersizer 2000 with a He-Ne laser (633 nm) and a blue solid-state light source (466 nm). The multi-zone detector provided a grain size spectrum from 0.02 µm to 2000 µm across 50 size classes. A Scirocco 2000 dry dispersion unit was employed for sample dispersion.

2.2.3. Measurement Procedure

Each aliquot was evenly spread as a triangular mound on a sample tray and processed with the following parameters: 8 mm dispersion slit width, 2 bar dispersion air pressure, and 50% tray vibration intensity. These settings ensured consistent sample flow. The LD analysis for each sample

Preprints.org (www.preprints.org) | NOT PEER-REVIEWED | Posted: 14 February 2025 doi:10.20944/preprints202502.1032.v1

involved three serial measurements, each consisting of 12,000 individual measurements over 12 seconds (i.e., device standard for one series).

2.2.4. LD Particle Size Analysis

Figure 1 presents the volume-based particle size distributions averaged from three sub-series of measurements for the two conducted series ("sample" and "duplicate") in the form of their relative distribution density "$q_3(x)$" and cumulative distribution curve "$Q_3(x)$", where "x" denotes the equivalent particle diameter determined in the analyses.

The two measured samples show very good agreement in particle characteristics across the entire measurement range. In the size range of approximately 300 – 600 µm, the density function for Sample 2 ("duplicate") exhibits a right shift compared to Sample 1, with its maximum slightly higher. However, both effects are negligible. For both measurements, a comparably broad particle size range (three orders of magnitude) from approximately 2 – 2000 µm is observed, with 80% of particles (i.e., the size range $x_{10,3}$ – $x_{90,3}$) falling between roughly 10 – 1000 µm (average for Sample 1: 12 – 886 µm, average for Sample 2: 13 – 913 µm). This range (spanning two orders of magnitude) should be considered for process design. The median ($x_{50,3}$) for both distributions is around an equivalent particle diameter of 300 µm (Sample 1: 280 µm, Sample 2: 302 µm), representing the typical particle size in the measured original sample.

Additionally, for process considerations, it is noteworthy that the left tail of the distribution extends over a broader range with a similar probability of occurrence (1 – 2% in the particle size classes between approximately 5 – 100 µm). This suggests that it may be beneficial to separate a fine fraction below 100 µm from the biochar before its use, potentially to remove interfering fine particles or create an additional "material type" for investigation of process behaviour.

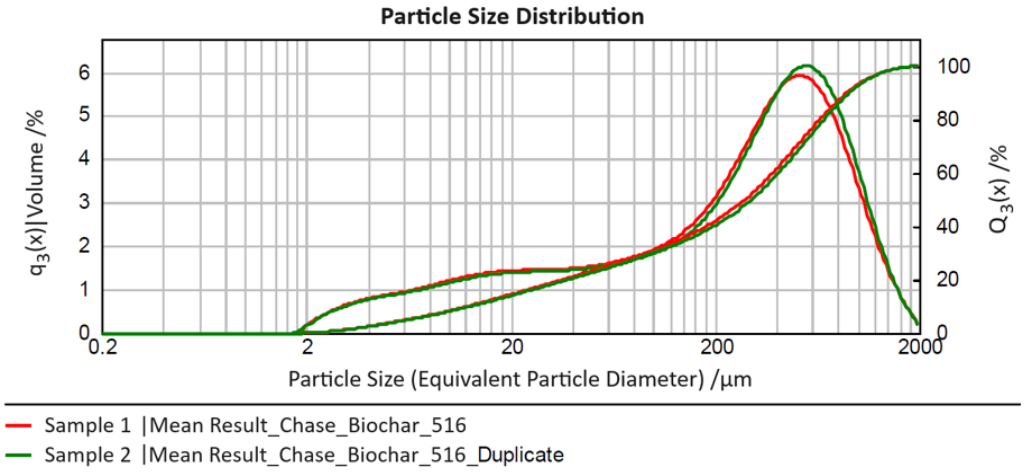

Figure 1. Mean particle size distributions by laser diffraction (LD) analysis of biochar.

2.3. Activation Process of Biochar to Activated Carbon

The chemical activation of raw biochar was performed using potassium hydroxide (KOH) as the activating agent. The impregnation ratio, defined as the weight ratio of KOH to biochar, was varied to assess its effect on the activation process. The ratios tested included 1:1, 2:1, and 3:1. For the activation, 200 mL of distilled water was first prepared, and the appropriate amount of KOH, ranging from 20 to 60 g, depending on the impregnation ratio, was dissolved in the water. After the KOH was fully dissolved, 20 g of raw biochar was added to the solution. The mixture was then stirred continuously for 5 hours. To further investigate the influence of stirring duration on the surface area, total pore volume, and other properties, the optimal impregnation ratio was also subjected to extended stirring periods of 12 and 24 hours.

Following impregnation, the mixtures were filtered and the resulting solids were dried until constant weight. The dried biochar samples were then subjected to carbonization. Each sample was

 doi:10.20944/preprints202502.1032.v1

placed in a quartz glass container, which was then positioned inside a stainless-steel reactor with dimensions of 300 mm in length and 20 mm in internal diameter. The reactor was heated in an electric furnace under a nitrogen atmosphere to prevent oxidation. Approximately 15 g of the impregnated material was loaded into each reactor. The samples were heated to final carbonization temperatures of 600 °C, 700 °C, 750 °C, and 800 °C at a heating rate of 10 °C/min, with a nitrogen flow rate of 300 mL/min. Upon reaching the target temperature, the samples were held at this temperature for one hour to complete the carbonization process. Following carbonization, the activated biochar samples were treated with 200 mL of 0.1 M hydrochloric acid (HCl) solution to remove any residual activating agent. After the acid treatment, the samples were thoroughly rinsed with distilled water until the pH of the wash water stabilized within a neutral range of 6-7. The final activated carbon products were then dried at 105 °C for 12 hours to ensure the complete removal of any remaining moisture. The yield of activated carbon is determined by dividing the dry weight of the resulting activated carbon by the dry weight of the original biochar and then multiplying the result by 100 to express it as a percentage.

$$\text{Yield (\%)} = \frac{(\text{Dry weight of activated carbon})}{(\text{Dry weight of biochar})} \times 100\% \quad (1)$$

Figure 2 illustrates the schematic process for the preparation of activated carbon samples.

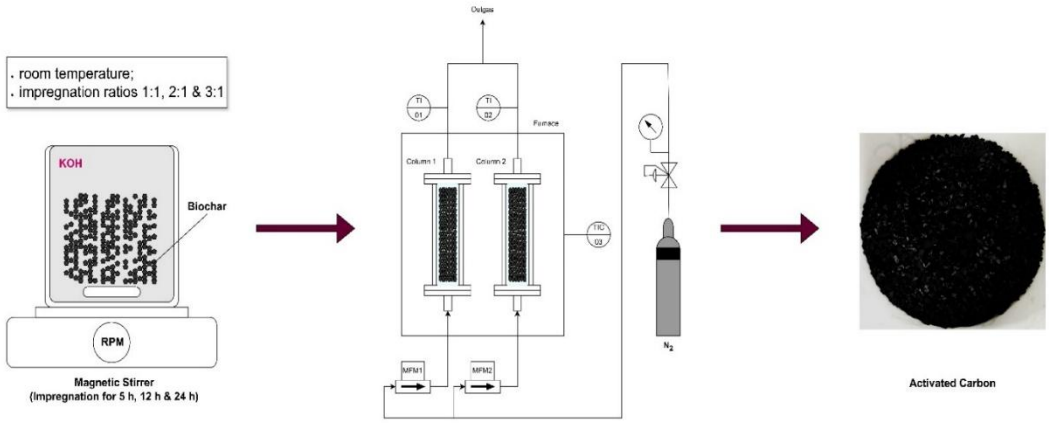

Figure 2. Process Overview: Activated Carbon Sample Preparation.

2.4. Sample Characterization

The raw biochar and activated carbon samples were degassed at less than 10 Pa and 300 °C for 2 hours using a Microtrac BELPREP II. The surface and pore characteristics were then analyzed through N_2 adsorption at 77 K using a BELSORP MAX X device, with measurements taken across a relative pressure range of 10^{-2} to 0.99 P/P_0. This data was used to calculate the pore size, pore volume, and surface area using Microtrac's BELMASTER software. The Brunauer-Emmet-Teller (BET) surface area was determined following the Rouquerol criteria, while pore size distributions were calculated using the NLDFT model for slit pores in carbon materials.

The morphology of the AC surface was determined using Scanning Electron Microscopy (SEM) using an FEI Quanta FEG250, with samples mounted on aluminum stubs using carbon tape. To enhance conductivity, samples were coated in a Q150T S sputter coater at 15 mA for 5-10 minutes. Elemental analysis was conducted by energy-dispersive X-ray spectroscopy (EDX) on the same microscope.

Fourier Transform Infrared (FTIR) spectroscopy was tested to determine surface functional groups. Spectra were monitored in the 4000 to 400 cm^{-1} range using a VERTEX 70 spectrometer, with 64 scans captured at a 2 cm^{-1} resolution.

 doi:10.20944/preprints202502.1032.v1

The efficiency of activated biochar is investigated through simultaneous thermal analysis (STA – TGA/DSC – Thermogravimetric Analysis with Differential Scanning Calorimetry) using a NETZSCH STA 449c TGA/DSC analyzer and NETZSCH Proteus software for data processing. The focus of the analysis was on the adsorption capabilities of the activated biochar for carbon dioxide (CO_2) diluted in an inert He gas stream (total gas flow rate 100 Nml/min) at a constant sample temperature of 30 °C. The sample size was ~20 mg in 6.8 mm Al_2O_3 crucibles. Various concentrations of CO_2 are employed to assess their impact on the adsorption process; a settling time of 20 min was introduced for reaching equilibrium at each concentration step. This approach aims to elucidate the relationship between CO_2 concentration and the adsorption efficiency of biochar, providing insights into its potential applications in carbon capture technologies.

3. Results

This section may be divided by subheadings. It should provide a concise and precise description of the experimental results, their interpretation, as well as the experimental conclusions that can be drawn.

3.1. Effects of KOH on the Yield of Activated Carbons

The yield of activated carbon derived from biochar through KOH activation was systematically examined under varying impregnation ratios of KOH to biochar 1:1, 2:1, and 3:1 and different activation temperatures at 600 °C, 700 °C, 750 °C, and 800 °C. As illustrated in Figure 3, both parameters significantly influenced the yield of the resulting activated carbon.

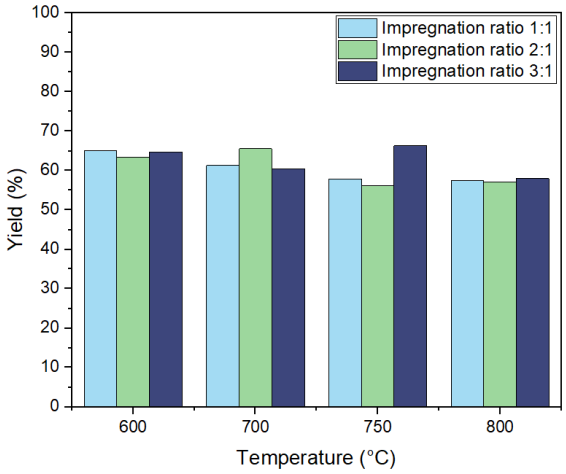

Figure 3. Yield of activated carbon from biochar using KOH activation at different impregnation ratios (1:1, 2:1, 3:1) and temperatures (600°C, 700°C, 750°C, 800°C).

It was found from previous research that increasing activation temperatures are typically accompanied by a decrease in the yield due to the release of volatile substances [35]. The yield of activated carbon ranged from 56.2% to 66.3%, reflecting relatively high values compared to similar findings in the literature. Higher activation temperatures, particularly at 800 °C, resulted in a general trend in the reduction in yield across all ratios due to the intensified burn-off of carbon. However, the elevated temperatures also facilitated a significant increase in BET surface area, indicating more effective micropore development. Specifically, for the 3:1 impregnation ratio at 800 °C, the BET surface area reached a peak value of 498 m^2/g, reflecting the enhanced microporosity resulting from the higher KOH concentration and elevated temperature, albeit with some carbon loss. Conversely, lower temperatures, such as 600 °C, yielded higher carbon recovery due to reduced burn-off, though this was not always accompanied by a maximal increase in BET surface area, as observed for the 2:1

 doi:10.20944/preprints202502.1032.v1

and 3:1 impregnation ratios. At 800 °C, the 3:1 impregnation ratio maintained a relatively high yield of 58%, suggesting that residual potassium may play a stabilizing role in preserving the carbon structure despite the aggressive activation conditions. In comparison to the literature, where the highest reported yield was 46.33% at 800 °C with a 1:1 ratio, the current study achieved a yield of 57.45% at the same temperature, indicating higher carbon retention under similar conditions [36].

For the 3:1 impregnation ratio, yields varied from 64.8% at 600 °C to 60.5% at 700 °C and peaked at 66.3% at 750 °C before declining to 58% at 800 °C. The observed trend aligns with literature reports suggesting that increasing the KOH-to-biochar ratio enhances yield. This enhancement can be related to potassium ions on the carbon surface acting as catalysts, accelerating the direct reaction between carbon and KOH, thereby promoting yield even at higher activation temperatures.

3.2. Surface Area and Pore Size Distribution

The surface area of activated carbon is measured using BET equipment BELSORP MAX X. This method uses nitrogen at 77 K to measure gas adsorption. BET analysis provides important information about the porosity and surface characteristics of the activated carbon.

The surface area is one of the important factors for determining the adsorption properties of activated carbon, as it directly relates to the ability of a material to adsorb different substances.
A higher BET surface area usually means there are more available adsorption sites, making the material more effective for gas and water purification applications. At an activation temperature of 600 °C, an increase in the impregnation ratio of KOH to biochar leads to a decrease in the surface area. However, at 800 °C, the surface area increases as the impregnation ratio increases. The change in surface area with the increase of the KOH to biochar impregnation ratio at different activation temperatures can be attributed to the varying chemical and physical processes that occur during the activation process. At 600 °C, the higher impregnation ratio may lead to a more pronounced chemical reaction or pore structure collapse, resulting in a decreased surface area.

In contrast, at 800 °C, the increase in impregnation ratio may promote the formation of more porous structures, leading to an increased surface area. These changes are influenced by the temperature and the chemical reactions during the activation process.

As illustrated in Figure 4, the surface area of activated carbon at 600 °C and 700 °C is greatest with an impregnation ratio of 1:1 (KOH: Biochar), followed by a ratio of 2:1, and is lowest at a ratio of 3:1. This decreasing in surface area at a 3:1 ratio indicates that a higher concentration of KOH may lead to an over-activation of the biochar, reducing its structural integrity and limiting pore formation. Conversely, the 2:1 ratio appears to provide a moderate level of activation that still promotes surface area but perhaps does not achieve the same efficiency as the 1:1 ratio at these temperatures. However, at 750 °C, a decrease in surface area is observed across all impregnation ratios. This may be due to excessive heat leading to the shrinkage of pores or the collapse of the biochar structure, diminishing the surface area.

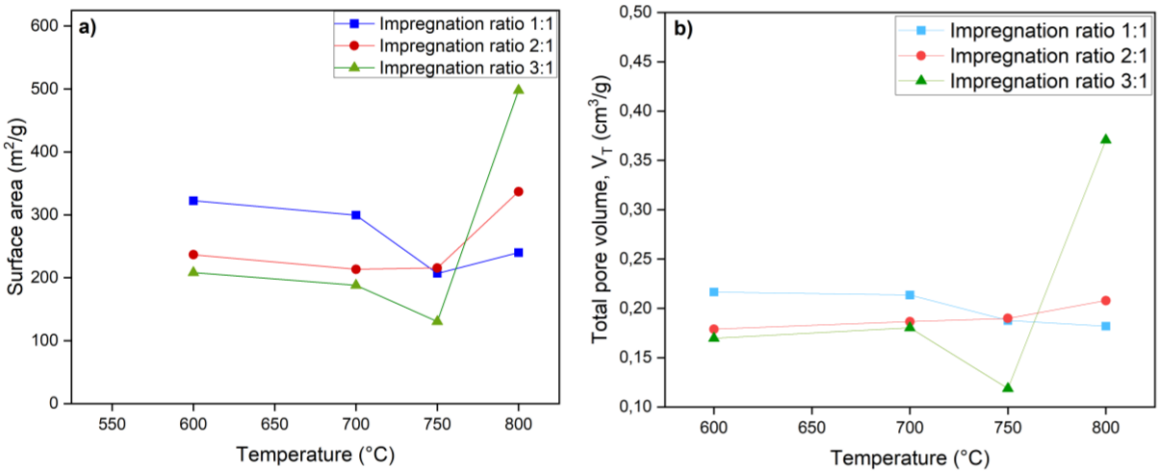

 doi:10.20944/preprints202502.1032.v1

(a) (b)

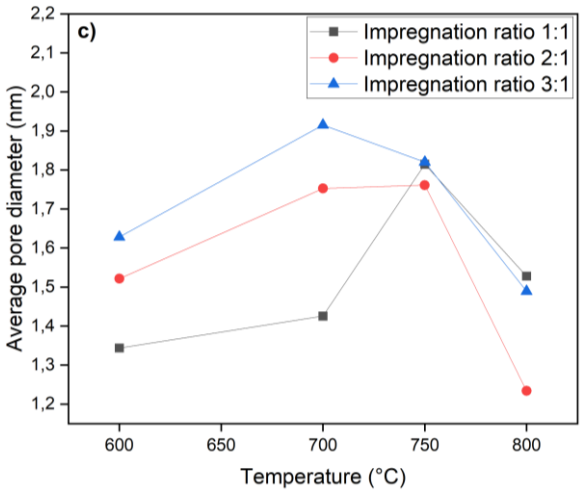

(c)

Figure 4. a) Influence the impregnation ratio and temperature on the surface area, b) total pore volume, and c) average pore size of activated carbon.

Interestingly, at 800 °C, the results reverse, showing an increase in surface area at the 3:1 ratio, with the average pore diameter decreasing, which indicates that higher temperatures can unlock new pore structures or facilitate different activation mechanisms that might not be present at lower temperatures. The results indicate that the impregnation ratio significantly influences the surface area of biochar at various carbonization temperatures.

The effect of time was examined at 5h, 12h, and 24h, as represented in Table 1. The optimal impregnation ratio for activated carbon was determined to be 3:1, processed at 800 °C for 24 hours. BET analysis of the activated carbon at this condition showed a specific surface area of 708 m^2/g, a total pore volume of 0.41 cm^3/g, and a pore size of 1.16 nm. The high specific surface area and microporous structure of the activated carbon indicate excellent potential for gas adsorption applications, particularly for CO_2 and CH_4. Compared to commercial activated carbons, the surface area is within the typical range (600–1,200), which confirms the efficiency of the chemical activation process of biochar.

Table 1. Influence of processing time on the surface area, total pore volume, and average pore size of activated carbon.

ACs	S_{BET} (m^2/g)	V_T (cm^3/g)	V_m (cm^3/g)	D_{pd} (nm)
Biochar	203	0.146	0.09	1.438
Impregnation ratio 3:1 (wt/wt)				
Activation temperature (°C)				
800	498	0.371	0.228	1.489
800 (12h)	590	0.362	0.286	1.228
800 (24h)	708	0.410	0.332	1.160

S_{BET}: BET surface area, V_T: total pore volume, V_m: mesopore volume, D_{pd}: average pore diameter.

 doi:10.20944/preprints202502.1032.v1

The adsorption isotherm was classified as Type I, which indicates a microporous structure, as shown in Figure 5. Micropores presence is along with the Type I isotherm, demonstrating strong adsorption capacity at low pressures, which is beneficial for energy storage and efficiency.

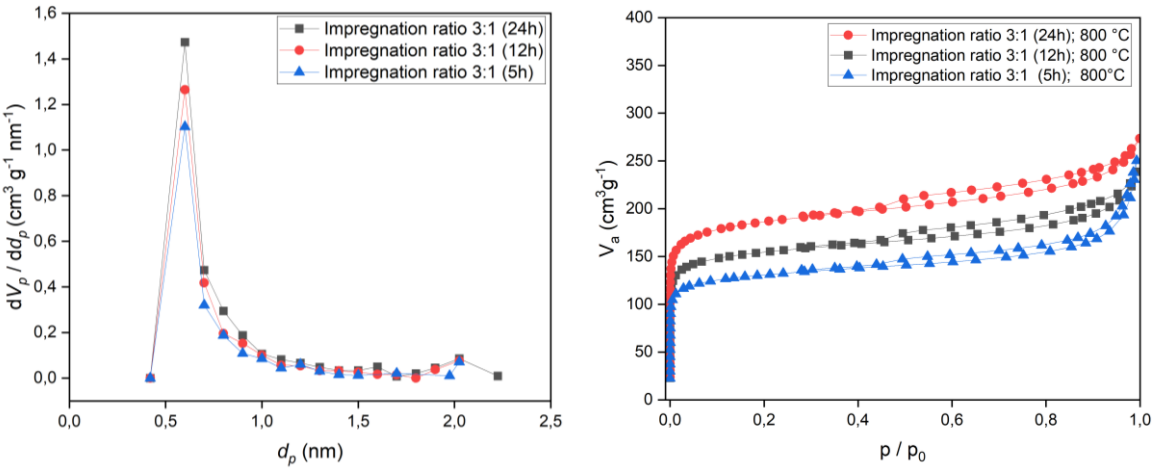

(**a**) (**b**)

Figure 5. Pore size distribution of activated carbon for an impregnation ratio of 3:1, with impregnation times of 5, 12, and 24 hours at an activation temperature of 800 °C. Additionally, adsorption/desorption isotherms corresponding to the same impregnation ratio and time intervals are presented, highlighting the influence of impregnation time on pore structure and adsorption characteristics.

3.3. Surface Functional Groups

FTIR was conducted to examine the surface functional groups of the chemically activated carbon samples. The spectra were recorded in the wavenumber range of 4000–400 cm^{-1}, as shown in Figure 6. The FTIR spectra for all activated carbon samples exhibit several characteristic peaks, which provide insights into the chemical transformations induced by KOH activation at various temperatures and impregnation ratios.

A broad, weak peak observed around 3700 cm^{-1} corresponds to the O-H stretching vibrations of hydroxyl groups [28,37]. The presence of these hydroxyl groups suggests that surface-bound hydroxyls are retained during the activation process, which likely contributes to the enhanced hydrophilicity of the activated carbon. In the range of 2900–2860 cm^{-1}, smaller peaks are visible, attributed to asymmetric C-H stretching vibrations representing methylene ($-CH_2$) and methyl($-CH_3$) groups [38,39]. These peaks indicate the presence of aliphatic chains, though their relatively low intensity suggests that these aliphatic compounds are not dominant functional groups on the activated carbon surface. A distinct peak at approximately 2347 cm^{-1} corresponds to the stretching vibrations of alkynes (C≡C) [3]. This peak is consistent across all impregnation ratios and temperatures, except for the sample activated at 800°C with a 3:1 impregnation ratio, as shown in Figure 6 (section b), where the band is significantly weaker. The reduction or absence of this peak at higher temperatures indicates a possible breakdown or gasification of triple bonds under extreme thermal conditions, particularly when higher KOH concentrations are used.

The peak observed at 1537 cm^{-1} is characteristic of C=C stretching vibrations, signaling the presence of aromatic rings in the carbon matrix [3,6]. This indicates that KOH activation facilitates the formation of stable aromatic structures, which are essential for the enhanced adsorption capacity and thermal stability of activated carbon. Furthermore, the wavenumber range between 1300 and 900 cm^{-1} corresponds to C-O stretching vibrations typically found in acids, phenols, esters, and alcohols, which are common in oxidized carbons [40,41]. These peaks are present across all impregnation ratios and temperatures but are notably smaller for samples treated at 700 °C and 600 °C with a 3:1 impregnation ratio, indicating a diminished presence of secondary alcohol or ether groups. The reduction in the intensity of these peaks at higher temperatures suggests that thermal activation

 doi:10.20944/preprints202502.1032.v1

reduces the oxygen-containing functional groups, potentially increasing hydrophobicity and improving pore structure. In contrast, for the 1:1 impregnation ratio, these peaks remain sharper across all temperatures, particularly at lower temperatures. Sharp peaks at 723 cm^{-1} and 655 cm^{-1} are attributed to C-H bending vibrations in benzene derivatives.

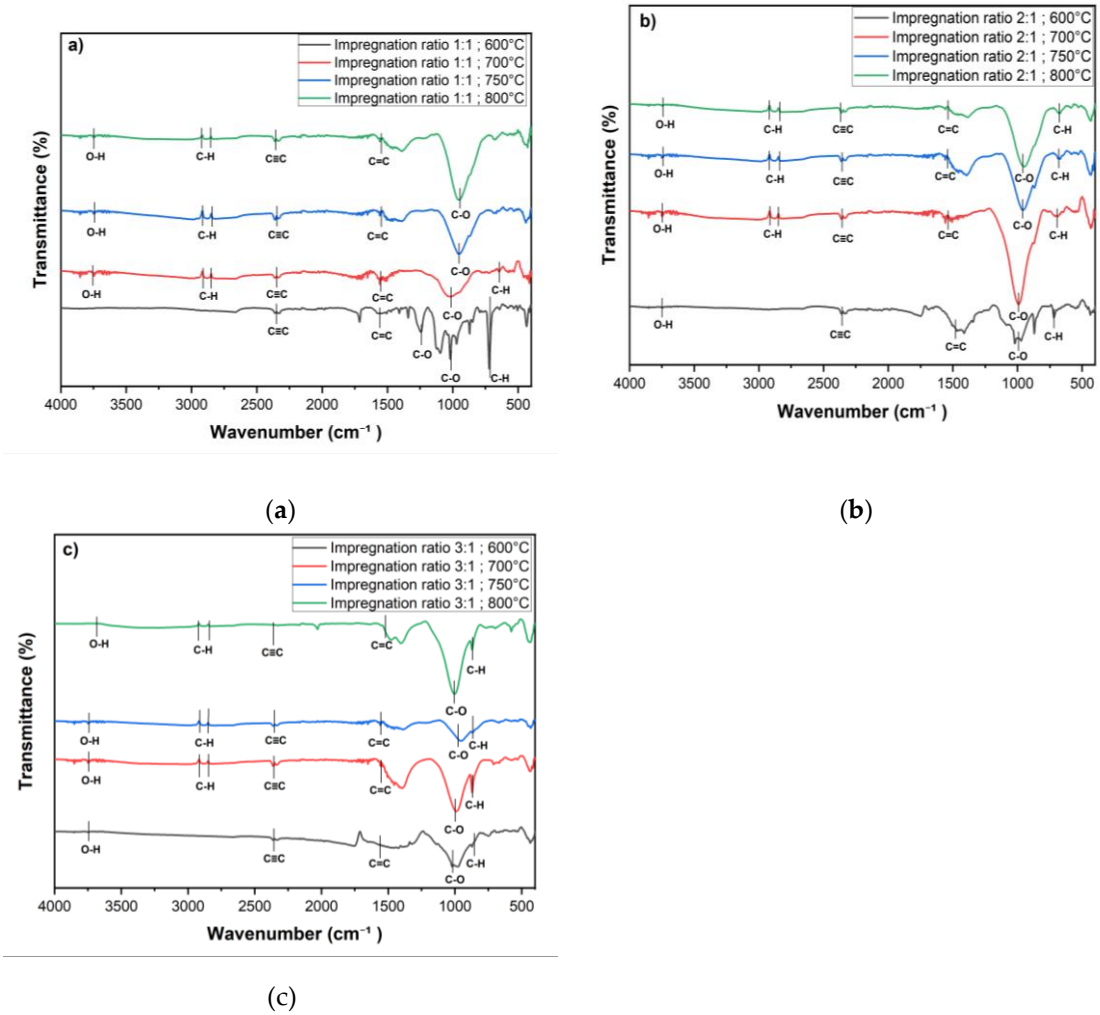

(**a**) (**b**)

(c)

Figure 6. FT-IR spectra of activated carbon at various impregnation ratios (1:1, 2:1, 3:1) and activation temperatures (600 °C, 700 °C, 750 °C, and 800 °C): a) 1:1 ratio, b) 2:1 ratio and c) 3:1 ratio.

The FTIR results represent that temperature and impregnation ratio play significant roles in determining the surface morphology of the activated carbon. The weakening or disappearance of specific functional groups at higher temperatures and impregnation ratios indicates the breakdown of volatile components, contributing to the overall structural modification of the activated carbon. The presence of hydroxyl groups contributes to increased hydrophilicity, while the stable aromatic structures enhance both the adsorption capacity and thermal stability. Higher temperatures result in the reduction of oxygen-containing functional groups, leading to improved pore structure and increased hydrophobicity. Besides, the formation of stable aromatic structures, as indicated by the presence of C=C stretching vibrations, enhances the adsorption capacity and thermal stability of the activated carbon.

3.4. Surface Morphology and EDX

The morphological analysis of the chemically activated carbon samples and the raw biochar was conducted using Scanning Electron Microscopy (SEM) to evaluate the impact of KOH activation. The SEM image in Figure 7a shows the untreated biochar, displaying a relatively rough surface texture with a visible porous structure, though small particles or impurities are present on the surface.

 doi:10.20944/preprints202502.1032.v1

High exothermic reactions are a consequence of the subsequent activation process, including the reaction of KOH with carbon/raw biochar at elevated temperatures. This significantly alters the structural morphology, as observed in Figures 7b to 7h. These images correspond to activation temperatures ranging from 600 °C to 800 °C. Figure 7b shows the activated carbon treated at 600 °C with an impregnation ratio of 1:1. The wall of the pores appears more refined compared to the raw biochar, with a noticeable increase in both the size and number of pores, indicating enhanced porosity. Despite that, some regions still exhibit residual particles or structures, which may be remnants of the original material or byproducts of the activation process. At an elevated temperature of 700 °C, the SEM image in Figure 7c reveals further refinement and smoothness of the pore walls, suggesting more advanced pore development. The increased activation temperature appears to contribute to the collapse of smaller pores while expanding larger ones, resulting in a modified pore size distribution and increased pore volume. Figure 7e illustrates the activated carbon at 800 °C with an impregnation ratio of 1:1, showing an even greater increase in pore volume. This phenomenon can be associated with the activation process with KOH, where the elevated energy input promotes a near-violent disintegration of the carbon matrix as KOH penetrates and intercalates within the structure [23]. This breakdown is further intensified by partial gasification due to the reactive oxygen released from the hydroxide. The mechanisms of KOH intercalation and subsequent "explosive" disintegration, coupled with gasification, likely account for the more developed porosity observed in the treated biochars compared to the untreated sample. In Figure 7f, the activation is again conducted at 800 °C, but with a higher impregnation ratio of 3:1. The morphology discloses a more heterogeneous pore structure comprising both mesopores and micropores. The diverse pore network enhances the material's ability to adsorb molecules of various sizes.

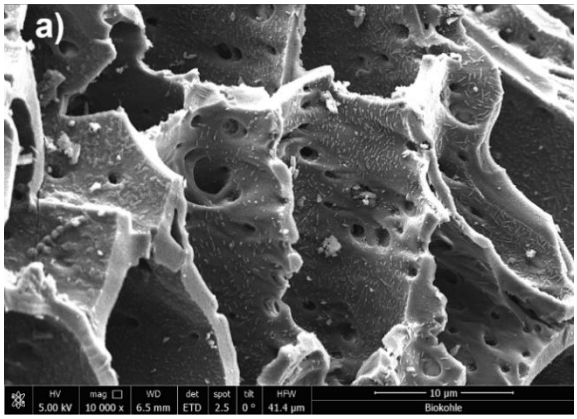

(**a**)

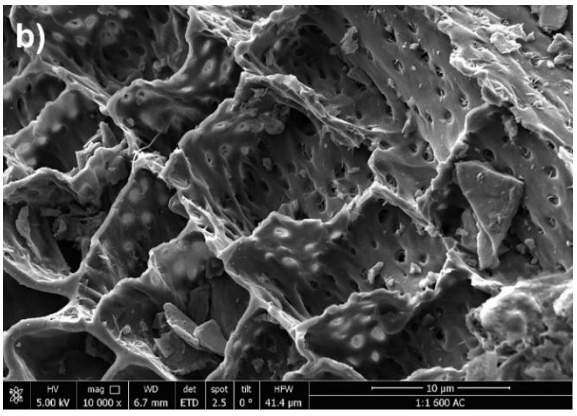

(**b**)

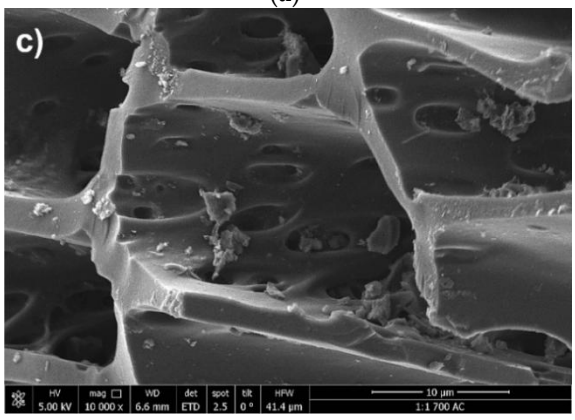

(**c**)

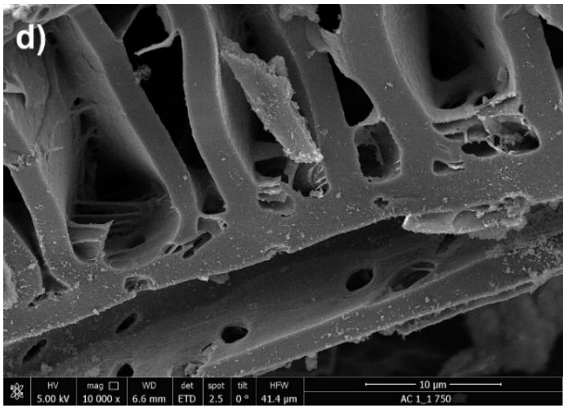

(**d**)

 doi:10.20944/preprints202502.1032.v1

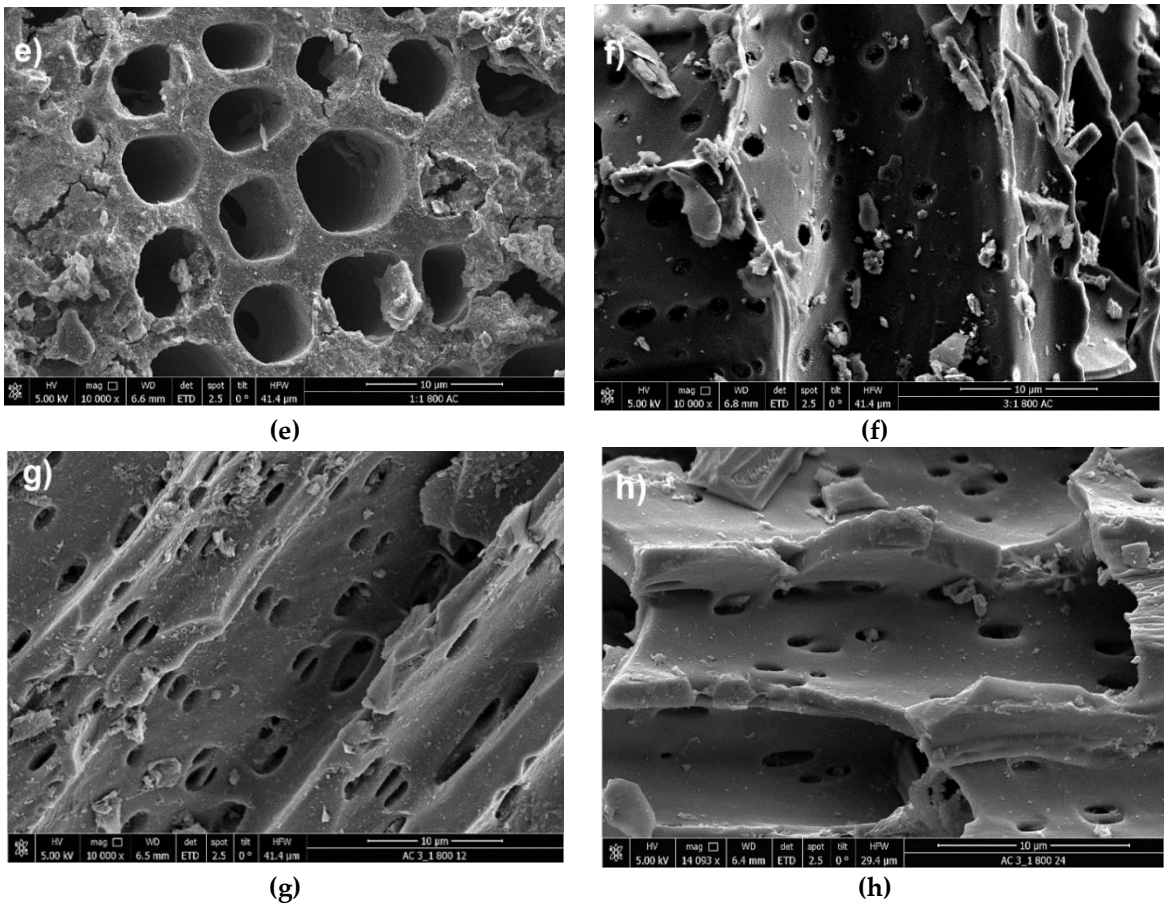

Figure 7. Surface morphology of biochar and activated carbon samples: (a) untreated biochar, (b)-(d) chemically activated carbon with an impregnation ratio of 1:1 at different activation temperatures—600 °C (b), 700 °C (c), and 800 °C (e), and (f) - (h) chemically activated biochar with an impregnation ratio of 3:1 at 800 °C for an activation time of 5 hours, 12 hours, and 24 hours.

The EDX analysis revealed substantial changes in the elemental composition of the biochar following chemical activation with KOH at 800 °C, using an impregnation ratio of 3:1 under a nitrogen atmosphere. In its untreated form, as shown in Figure 8a, the biochar predominantly consisted of carbon, comprising 73.9% of the total mass, indicative of its organic nature, with oxygen accounting for 16.1%. Upon activation, as depicted in Figure 8b, the carbon content declined to 61.4%, likely due to partial oxidation and gasification processes at elevated temperatures, which resulted in the release of carbon species such as CO and CO_2. Although carbon is reduced, the remaining carbon has the potential to enhance the structural morphology and adsorption performance of the activated carbon. This potential is due to the predicted exhibition of an elevated degree of graphitization and thermal stability.

The increase in oxygen content to 19.0% after activation suggests the formation of oxygen-containing functional groups, such as hydroxyl and carboxyl groups, this can also be observed in the FTIR analysis, Figure 6. These functional groups enhance the adsorption properties of the biochar by providing active sites for polar interactions and chemical reactions. The results indicated potassium enrichment from 1.5% to 7.6%, implying the incorporation of potassium compounds, such as potassium carbonate, originating from the KOH used during activation [35]. The significantly higher BET surface area observed at 800 °C (498 m^2/g) infers the effective development of a porous structure and elucidates that this incorporation plays a pivotal role in promoting pore formation. The detection of chlorine in the activated carbon, which was absent in the untreated sample, can be attributed to residual chlorine from the post-activation washing step with hydrochloric acid (HCl). In the experimental procedure, the activated carbon samples were washed with a solution composed of 0.1 M HCl to remove residual activating agents, followed by thorough rinsing with distilled water

 doi:10.20944/preprints202502.1032.v1

until the pH stabilized within a neutral range. The presence of chlorine suggests that traces of the acid treatment may have remained, despite the rinsing process.

Although it is well-documented that acid washing with HCl [42] can effectively remove inorganic elements from carbon materials, the EDX results showed that certain inorganic elements, such as potassium, silicon, and aluminum, were still present in the activated biochar. This indicates that while the acid treatment successfully eliminated some components, such as gold (Au), palladium (Pd), and iron (Fe), which were detected in the untreated biochar, other elements may have been retained due to their incorporation into the carbon structure during activation or the formation of stable compounds that were less susceptible to removal by the acid washing process.

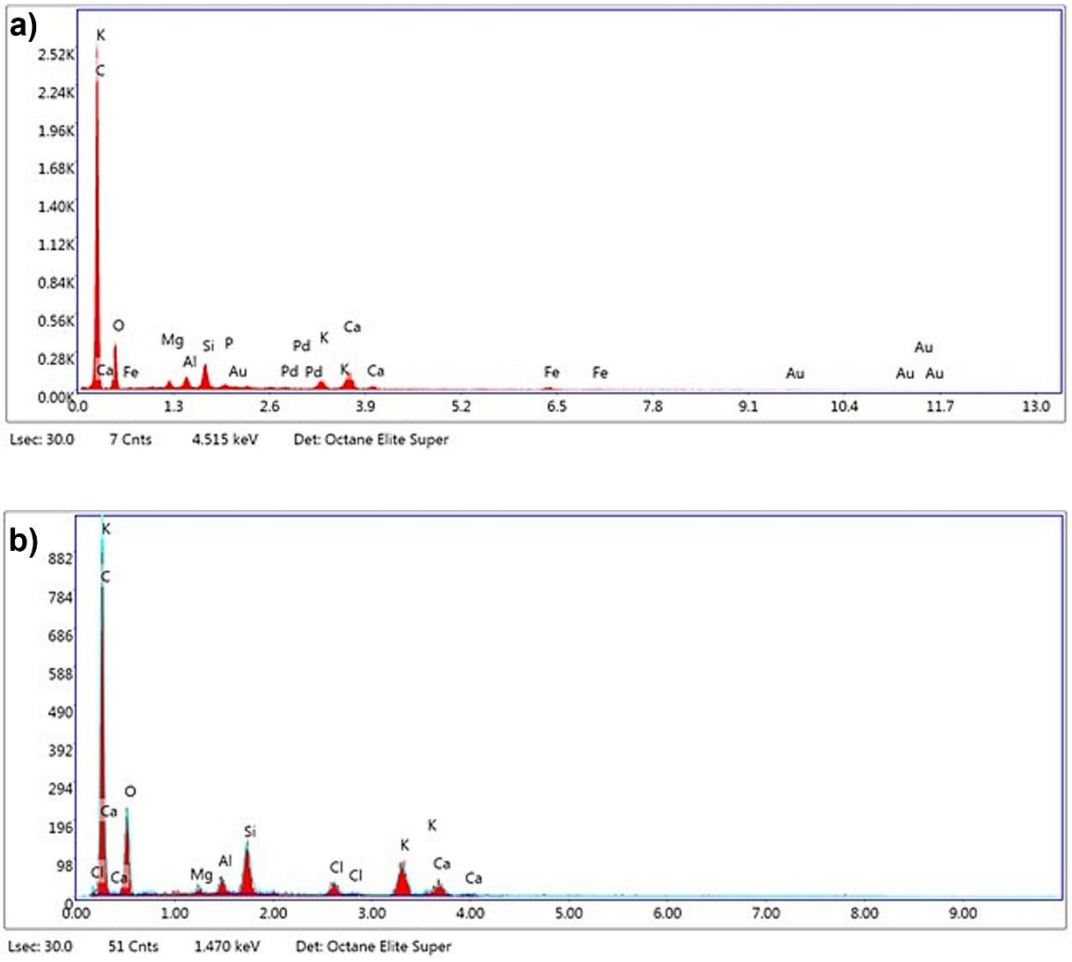

Figure 8. EDX spectra of a) biochar before chemical activation with KOH and b) biochar after chemical activation with KOH at 800 °C with an impregnation ratio of 3:1.

The observed changes in elemental composition, increased oxygen content, and surface enrichment with potassium prove that the activation process produced a high-quality activated carbon with improved surface chemistry and porosity. These modifications make the biochar suitable for adsorption applications, validating the effectiveness of the chemical activation and post-treatment methods employed in this study.

3.5. STA (TGA/DSC)

The Differential Scanning Calorimetry (DSC) analysis of raw and activated biochar was conducted systematically to evaluate their adsorption performance across various CO_2 concentrations, focusing on the impact of activation on enhancing this performance. A mixture of CO_2 and He was introduced to biochar and activated carbon at flow rates of 5, 10, 15, 20, 40, and 75

 doi:10.20944/preprints202502.1032.v1

% at a temperature of 30 °C. The DSC analysis reveals that the thermal behavior of raw biochar is less pronounced compared to that of activated biochar. The activation process carried out under controlled conditions—specifically at 800 °C with a 3:1 impregnation ratio for 24 hours—resulted in a substantial improvement in CO_2 adsorption properties, as shown in Figure 9. Notably, the area of the adsorption peak for CO_2 at 30 °C increased by approximately 34% post-activation, as detailed in Table 2.

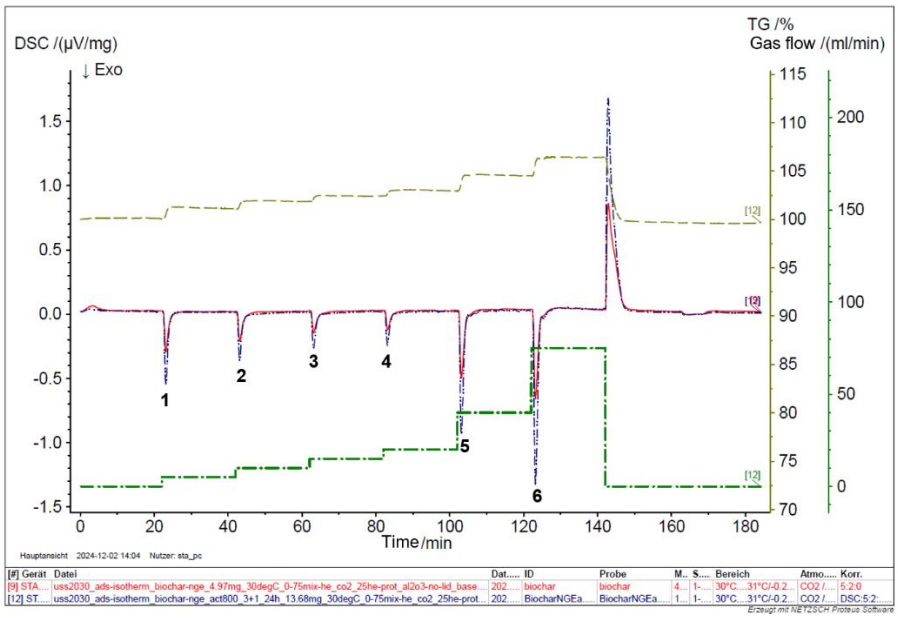

Figure 9. DSC analysis of biochar and activated carbon.

Compared to raw biochar, the enhanced CO_2 adsorption performance by activated biochar can be primarily attributed to the activation process. Activated biochar features a significantly larger surface area (709 m^2/g versus 200.3 m^2/g), providing more gas adsorption sites. Also, the activation process produced a more intricate pore structure, including mesopores and micropores, thereby improving the ability of the material to trap gases. Moreover, activated biochar mainly has a lower ash content, which helps maximize the effective surface area available for adsorption. These factors collectively improve the physicochemical properties of activated biochar, making it a more effective material for CO_2 gas adsorption, as evidenced by increased adsorption peak areas observed in DSC analysis.

Table 2. DSC Results at different CO_2 concentrations.

Peak No	Modus	Temperature (°C)	CO_2 %	He_2 % (protect)	He_2 % (purge)	DSC Biochar (µV/mg)	DSC Activated (µV/mg)
1.	isotherm	30.5	5	70	25	-24.19	-35.37
2.	isotherm	30.5	10	65	25	-19.64	-25.47
3.	isotherm	30.5	15	60	25	-14.87	-19.91
4.	isotherm	30.5	20	55	25	-12.09	-18.59
5.	isotherm	30.5	40	35	25	-41.14	-63.73
6.	isotherm	30.5	75	0	25	-55.04	-94.38

4. Discussion

This study explores the importance of utilizing renewable biomass sources, not only as an efficient and economical alternative for the production of activated carbon but also as a way to

 doi:10.20944/preprints202502.1032.v1

contribute to environmental sustainability. This research emphasizes the promising potential of biochar produced from sunflower seed shells as a sustainable precursor for activated carbon production through KOH activation.

In particular, the research was conducted to optimize biochar conversion to activated carbon via KOH. Various activation parameters were examined, including the KOH/biochar impregnation ratios (1:1, 2:1, 3:1) and activation temperatures (600 °C, 700 °C, 750 °C, 800 °C) over different durations (5 hours, 12 hours, and 24 hours). A high yield of approximately 66.3% of activated carbon was achieved at 750 °C with an impregnation ratio of 3:1.

The optimal impregnation ratio for activated biochar was found to be 3:1, processed at 800 °C for 24 hours. BET analysis under these conditions revealed a specific surface area of 708 m^2/g, a total pore volume of 0.41 cm^3/g, and an average pore size of 1.16 nm, indicating significant potential for high adsorption capacity. This substantial surface area enhances its efficiency in adsorbing various pollutants like CO_2, making it a valuable source for multiple applications. Considering all of this, we were able to demonstrate a feasible process using biochar as a sustainable resource to obtain high-quality activated carbon.

Author Contributions: Conceptualization, Selma Kuloglija; methodology, Selma Kuloglija; validation, Selma Kuloglija, and Amal Ahmed El Gohary; formal analysis, Selma Kuloglija, Wolfgang Impsmiller, Noah Steinacher, and Christian Jordan; investigation, Selma Kuloglija, Amal Ahmad El Gohary, and Christian Jordan; resources, Angelika Luckeneder and Daniela Meitner; data curation, Selma Kuloglija; writing—original draft preparation, Selma Kuloglija; writing—review and editing, Amal Ahmed El Gohary and Franz Winter; visualization, Selma Kuloglija; supervision, Amal Ahmed El Gohary, Christian Jordan, Franz Winter and Michael Harasek. All authors have read and agreed to the published version of the manuscript.

Funding: "This research received no external funding".

Data Availability Statement: We encourage all authors of articles published in MDPI journals to share their research data. In this section, please provide details regarding where data supporting reported results can be found, including links to publicly archived datasets analyzed or generated during the study. Where no new data were created, or where data is unavailable due to privacy or ethical restrictions, a statement is still required. Suggested Data Availability Statements are available in section "MDPI Research Data Policies" at https://www.mdpi.com/ethics.

Acknowledgments: The authors would like to express their gratitude to Sonnenerde GmbH and Next Generation Elements GmbH for providing the biochar. Additionally, they would like to thank TU Wien for granting access to the analytical instruments used to measure the properties of the activated carbon and the TU Wien Library for OpenAccess-Funding. The authors also acknowledge CS Odessa for their support and for granting permission to use ConceptDraw in creating graphical abstracts and other visuals utilized in this publication.

Conflicts of Interest: The authors declare no conflicts of interest.

Abbreviations

The following abbreviations are used in this manuscript:

AC	Activated carbon
KOH	Potassium hydroxide
CO_2	Carbon dioxide
$ZnCl_2$	Zinc chloride
H_3PO_4	Phosphoric acid
NaOH	Sodium hydroxide
H_2SO_4	Sulfuric acid
K_2CO_3	Potassium carbonate
K_2O	Potassium oxide

 doi:10.20944/preprints202502.1032.v1

K	Potassium
N_2	Nitrogen
NGE	Next Generation Elements
LD	Laser diffraction
BET	Brunauer-Emmet-Teller
SEM	Scanning Electron Microscopy
EDX	Energy-dispersive X-ray
FTIR	Fourier Transform Infrared
STA	Simultaneous Thermal Analysis
TGA	Thermogravimetric Analysis
DSC	Differential Scanning Calorimetry
CH_4	Methane
S_{BET}	BET Surface Area
V_T	Total Pore Volume
V_m	Mesopore Volume
D_{pd}	Avarage Pore Diameter

References

1. M. Şirazi and S. Aslan, 'Comprehensive characterization of high surface area activated carbon prepared from olive pomace by KOH activation', *Chem Eng Commun*, vol. 208, no. 10, pp. 1479–1493, 2021, doi: 10.1080/00986445.2020.1864628.
2. T. E. Amakoromo, O. E. Abumere, and J. A. Amusan, 'Synthesis and characterization of a high surface area activated carbon derived from cassava peels waste by KOH activation', *Scientia Africana*, vol. 20, no. 3, pp. 141–148, Jan. 2022, doi: 10.4314/sa.v20i3.12.
3. E. M. Mistar, T. Alfatah, and M. D. Supardan, 'Synthesis and characterization of activated carbon from Bambusa vulgaris striata using two-step KOH activation', *Journal of Materials Research and Technology*, vol. 9, no. 3, pp. 6278–6286, 2020, doi: 10.1016/j.jmrt.2020.03.041.
4. A. Fletcher, T. Somorin, and O. Aladeokin, 'Production of High Surface Area Activated Carbon from Peanut Shell by Chemical Activation with Zinc Chloride: Optimisation and Characterization', *Bioenergy Res*, vol. 17, no. 1, pp. 467–478, Mar. 2024, doi: 10.1007/s12155-023-10683-7.
5. Y. Yao *et al.*, 'Efficient dye adsorption of mesoporous activated carbon from bamboo parenchyma cells by phosphoric acid activation', *RSC Adv*, vol. 14, no. 18, pp. 12873–12882, Apr. 2024, doi: 10.1039/d4ra01652a.
6. Awitdrus *et al.*, 'KOH activation with microwave irradiation and its effect on the physical properties of orange peel activated carbon', in *Journal of Physics: Conference Series*, IOP Publishing Ltd, Oct. 2021. doi: 10.1088/1742-6596/2049/1/012025.
7. M. Corral-Bobadilla, R. Lostado-Lorza, F. Somovilla-Gómez, and R. Escribano-García, 'Effective use of activated carbon from olive stone waste in the biosorption removal of Fe(III) ions from aqueous solutions', *J Clean Prod*, vol. 294, Apr. 2021, doi: 10.1016/j.jclepro.2021.126332.
8. M. J. Saad *et al.*, 'Physical and chemical properties of the rice straw activated carbon produced from carbonization and KOH activation processes', *Sains Malays*, vol. 48, no. 2, pp. 385–391, Feb. 2019, doi: 10.17576/jsm-2019-4802-16.
9. M. Ruiz-Ojeda, L. Fonseca, and E. Amado-González, 'Optimization of activated carbon production from chicken manure by chemical activation with KOH and H3PO4', *Chem Eng Trans*, vol. 50, pp. 115–120, 2016, doi: 10.3303/CET1650020.
10. S. P. Galinato, J. K. Yoder, and D. Granatstein, 'The economic value of biochar in crop production and carbon sequestration', *Energy Policy*, vol. 39, no. 10, pp. 6344–6350, Oct. 2011, doi: 10.1016/j.enpol.2011.07.035.
11. M. B. Ahmed, J. L. Zhou, H. H. Ngo, and W. Guo, 'Insight into biochar properties and its cost analysis', Jan. 01, 2016, *Elsevier Ltd*. doi: 10.1016/j.biombioe.2015.11.002.
12. T. A. Kurniawan *et al.*, 'Challenges and opportunities for biochar to promote circular economy and carbon neutrality', *J Environ Manage*, vol. 332, Apr. 2023, doi: 10.1016/j.jenvman.2023.117429.

13. M. Gale, T. Nguyen, M. Moreno, and K. L. Gilliard-Abdulaziz, 'Physiochemical Properties of Biochar and Activated Carbon from Biomass Residue: Influence of Process Conditions to Adsorbent Properties', *ACS Omega*, vol. 6, no. 15, pp. 10224–10233, Apr. 2021, doi: 10.1021/acsomega.1c00530.
14. X. Tan *et al.*, 'Application of biochar for the removal of pollutants from aqueous solutions', Apr. 01, 2015, *Elsevier Ltd*. doi: 10.1016/j.chemosphere.2014.12.058.
15. H. Li, X. Dong, E. B. da Silva, L. M. de Oliveira, Y. Chen, and L. Q. Ma, 'Mechanisms of metal sorption by biochars: Biochar characteristics and modifications', 2017, *Elsevier Ltd*. doi: 10.1016/j.chemosphere.2017.03.072.
16. K. Jedynak and B. Charmas, 'Adsorption properties of biochars obtained by KOH activation', *Adsorption*, vol. 30, no. 2, pp. 167–183, Feb. 2024, doi: 10.1007/s10450-023-00399-7.
17. N. Khan, P. Chowdhary, E. Gnansounou, and P. Chaturvedi, 'Biochar and environmental sustainability: Emerging trends and techno-economic perspectives', Jul. 01, 2021, *Elsevier Ltd*. doi: 10.1016/j.biortech.2021.125102.
18. M. Sevilla and R. Mokaya, 'Energy storage applications of activated carbons: Supercapacitors and hydrogen storage', in *Energy and Environmental Science*, Royal Society of Chemistry, 2014, pp. 1250–1280. doi: 10.1039/c3ee43525c.
19. S. V Mikhalovsky and V. G. Nikolaev, 'Activated Carbon Surfaces in Environmental Remediation Activated carbons as medical adsorbents'.
20. D. A. Saputra, A. Pratoto, M. F. Rahman, and A. Kodama, 'THE EFFECT OF CHEMICAL ACTIVATION AGENTS AND ACTIVATION TEMPERATURE ON THE PORE STRUCTURE OF RICE HUSK-DERIVED ACTIVATED CARBON', *Malaysian Journal of Science*, vol. 43, no. sp1, pp. 1–7, Jul. 2024, doi: 10.22452/mjs.vol43sp1.1.
21. H. Arslanoğlu, 'Direct and facile synthesis of highly porous low cost carbon from potassium-rich wine stone and their application for high-performance removal', *J Hazard Mater*, vol. 374, pp. 238–247, Jul. 2019, doi: 10.1016/j.jhazmat.2019.04.042.
22. Ö. Şahin and C. Saka, 'Preparation and characterization of activated carbon from acorn shell by physical activation with H2O-CO2 in two-step pretreatment', *Bioresour Technol*, vol. 136, pp. 163–168, 2013, doi: 10.1016/j.biortech.2013.02.074.
23. R. Nedjai, N. A. Kabbashi, M. Z. Alam, and M. F. R. Al-Khatib, 'Production and Characterization of Activated Carbon from Baobab Fruit Shells by Chemical Activation Using ZnCl2, H3PO4 and KOH', in *Journal of Physics: Conference Series*, IOP Publishing Ltd, Dec. 2021. doi: 10.1088/1742-6596/2129/1/012009.
24. S. K. Shahcheragh, M. M. Bagheri Mohagheghi, and A. Shirpay, 'Effect of physical and chemical activation methods on the structure, optical absorbance, band gap and urbach energy of porous activated carbon', *SN Appl Sci*, vol. 5, no. 12, Dec. 2023, doi: 10.1007/s42452-023-05559-6.
25. C. F.-G. A. M.-G. V. G.-S. M.Olivares-Marin, 'Preparation of activated carbon from cherry stones by chemical activation with ZnCl2'.
26. S. Yorgun, N. Vural, and H. Demiral, 'Preparation of high-surface area activated carbons from Paulownia wood by ZnCl2 activation', *Microporous and Mesoporous Materials*, vol. 122, no. 1–3, pp. 189–194, Jun. 2009, doi: 10.1016/j.micromeso.2009.02.032.
27. L. Muniandy, F. Adam, A. R. Mohamed, and E. P. Ng, 'The synthesis and characterization of high purity mixed microporous/mesoporous activated carbon from rice husk using chemical activation with NaOH and KOH', *Microporous and Mesoporous Materials*, vol. 197, pp. 316–323, 2014, doi: 10.1016/j.micromeso.2014.06.020.
28. A. Kumar and H. M. Jena, 'Preparation and characterization of high surface area activated carbon from Fox nut (Euryale ferox) shell by chemical activation with H3PO4', *Results Phys*, vol. 6, pp. 651–658, 2016, doi: 10.1016/j.rinp.2016.09.012.
29. S. Yorgun and D. Yildiz, 'Preparation and characterization of activated carbons from Paulownia wood by chemical activation with H3PO4', *J Taiwan Inst Chem Eng*, vol. 53, pp. 122–131, Aug. 2015, doi: 10.1016/j.jtice.2015.02.032.

30. Yuliusman, F. Al Farouq, S. P. Sipangkar, M. Fatkhurrahman, and S. A. Putri, 'Preparation and characterization of activated carbon from corn stalks by chemical activation with KOH and NaOH', in *AIP Conference Proceedings*, American Institute of Physics Inc., Sep. 2020. doi: 10.1063/5.0014403.
31. K. Hussaro, 'PREPARATION OF ACTIVATED CARBON FROM PALM OIL SHELL BY CHEMICAL ACTIVATION WITH Na 2 CO 3 AND ZnCl 2 AS IMPRENATED AGENTS FOR H 2 S ADSORPTION', *Am J Environ Sci*, vol. 10, no. 4, pp. 336–346, 2014, doi: 10.3844/ajessp.2014.
32. M. J. Martin, M. D. Balaguer, and M. Rigola, 'Feasibility of activated carbon production from biological sludge by chemical activation with zncl2 and h2so4', *Environmental Technology (United Kingdom)*, vol. 17, no. 6, pp. 667–671, Jun. 1996, doi: 10.1080/09593331708616433.
33. W. Wu, C. Wu, G. Zhang, J. Liu, Y. Li, and G. Li, 'Synthesis and characterization of magnetic K2CO3-activated carbon produced from bamboo shoot for the adsorption of Rhodamine b and CO2 capture', *Fuel*, vol. 332, Jan. 2023, doi: 10.1016/j.fuel.2022.126107.
34. O. Oginni, K. Singh, G. Oporto, B. Dawson-Andoh, L. McDonald, and E. Sabolsky, 'Influence of one-step and two-step KOH activation on activated carbon characteristics', *Bioresour Technol Rep*, vol. 7, Sep. 2019, doi: 10.1016/j.biteb.2019.100266.
35. M. Tsarpali, J. N. Kuhn, and G. P. Philippidis, 'Activated carbon production from algal biochar: Chemical activation and feasibility analysis', *Fuel Communications*, vol. 19, p. 100115, Jun. 2024, doi: 10.1016/j.jfueco.2024.100115.
36. Abechi S E, Gimba C E, and U. A. Dallatu, 'Preparation and Characterization of Activated Carbon from Palm Kernel Shell by Chemical Activation', 2013. [Online]. Available: www.isca.in
37. W. Thongpat, J. Taweekun, and K. Maliwan, 'Synthesis and characterization of microporous activated carbon from rubberwood by chemical activation with KOH', *Carbon Letters*, vol. 31, no. 5, pp. 1079–1088, Oct. 2021, doi: 10.1007/s42823-020-00224-z.
38. M. B. Hay and S. C. B. Myneni, 'Structural environments of carboxyl groups in natural organic molecules from terrestrial systems. Part 1: Infrared spectroscopy', *Geochim Cosmochim Acta*, vol. 71, no. 14, pp. 3518–3532, Jul. 2007, doi: 10.1016/j.gca.2007.03.038.
39. 'silverstein-bassler-1962-spectrometric-identification-of-organic-compounds'.
40. S. Garba, O. A. Babatunde, S. Garba, and Z. N. Ali, 'Surface Modification of Activated Carbon for Improved Iodine and Carbon Tetrachloride Adsorption', *American Journal of Chemistry*, vol. 6, no. 3, pp. 74–79, 2016, doi: 10.5923/j.chemistry.20160603.02.
41. Z. Lendzion-Bieluń *et al.*, 'Surface characteristics of KOH-treated commercial carbons applied for CO2 adsorption', *Adsorption Science and Technology*, vol. 36, no. 1–2, pp. 478–492, Feb. 2018, doi: 10.1177/0263617417704527.
42. N. Karakehya, 'Effects of one-step and two-step KOH activation method on the properties and supercapacitor performance of highly porous activated carbons prepared from Lycopodium clavatum spores', *Diam Relat Mater*, vol. 135, May 2023, doi: 10.1016/j.diamond.2023.109873.